Journal of Photochemistry & Photobiology, A: Chemistry 404 (2021) 112955

Contents lists available at ScienceDirect

Journal of Photochemistry & Photobiology, A: Chemistry

journal homepage: www.elsevier.com/locate/jphotochem

Photodegradation of pollutant pesticide by oxidized graphitic carbon nitride catalysts

Shibiru Yadeta Ejeta [a], Toyoko Imae [a,b,c,*]

[a] Graduate Institute of Applied Science and Technology, National Taiwan University of Science and Technology, Keelung Road, Taipei, 10607, Taiwan, ROC
[b] Department of Chemical Engineering, National Taiwan University of Science and Technology, Keelung Road, Taipei, 10607, Taiwan, ROC
[c] Department of Materials Science and Engineering, National Taiwan University of Science and Technology, Keelung Road, Taipei, 10607, Taiwan, ROC

ARTICLE INFO

Keywords:
Oxidized graphitic carbon nitride
Graphitic carbon nitride
Photocatalytic degradation
Pollutant pesticide
2,4-Diphenoxyacetic acid

ABSTRACT

Oxygen-doped graphitic carbon nitride (Og-CN) was synthesized by H_2O_2-treating of graphitic carbon nitride (g-CN), which was prepared by the condensation-polymerization of melamine and the exfoliation. The successful oxidation was confirmed by the decrease of photoluminescence intensity, the detection of oxygen-including bond and the slight increase of surface area. Og-CN was applied to the photocatalytic degradation of 2,4-dichlorophenoxyacetic acid in the aqueous phase under the UV and visible light irradiation and compared with the catalytic behavior of g-CN. The degradation efficiency of Og-CN was higher than that of g-CN, the UV light irradiation was more effective than the visible light irradiation, and Og-CN was stable in three photocatalytic cycles with only 4% decrease. The kinetics analysis indicated that the photoreactions of both Og-CN and g-CN follow the zeroth-order reaction rather than the first-order reaction. On the photoreaction mechanism study, the active species-trapping experiment, which was performed using 2,2,6,6-tetramethyl-1-piperdinyloxy free radical, t-BuOH and KI for scavenging $O_2^{\bullet -}$, $O^{\bullet}H$ and h^+, respectively, confirmed the reactivity order of $O_2^{\bullet -} > {}^{\bullet}OH > h^+$. Then the present research refers that Og-CN is a promising photocatalyst because it has extremely high total organic carbon removal (88 % of degraded 2,4-D after 120 min).

1. Introduction

Environmental pollutions by organic and organometallic compounds are drastically rising and becoming a serious problem from time to time all around the world [1–3]. This rapidly increased issue may be attributed to industrialization, urbanization and agricultural expansion. Specifically, the recent attention is that along with the intense agricultural demand, the amount of pesticides and/or herbicides administrated in agricultural works remarkably increases and it is a strong risk to human health [4,5]. Among organic chlorine pesticides, the most common one is 2,4-dichlorophenoxyacetic acid (2,4-D), which is used in the whole world, specifically, in the developing countries [6,7]. It is a non-biodegradable aromatic herbicide utilized to damage broad leaves from weeds, and thus its residue may admix in soil-borne and water bodies and becomes the environmental hazard. The World Health Organization classifies 2,4-D as a mildly toxic chemical and the maximum tolerable amount in drinking water is 100 ppb [8–10]. Thus, the development of appropriate treatments is necessary to maintain this condition. Among many treatments, filtration, adsorption, coagulation, and ion exchange methods have been explored to remove 2,4-D from water systems [11,12]. However, those treatments should be forced the resumption of 2,4-D and/or provide excess secondary chemical pollutants that can affect the environments.

Photocatalytic degradation is a more promising technique, because it actively uses renewable solar energy to change harmful pollutants to harmless products without using other oxidative chemicals [13,14]. In these cases, metal oxide or metal semiconductor catalysts have generally been used, although they are less abundant and toxic in some cases [15,16]. Graphitic carbon nitride (g-CN) is a metal-free material consisting of the most abundant elements (carbon and nitrogen) and easily synthesized by the condensation polymerization of nitrogen-rich compounds such as thiourea, urea, cyanamide, dicyandiamide and melamine [17–19]. It is one of the most promising photocatalysts because of its stability, non-toxicity, tunability, reusability, flexible layer formability and small bandgap (about 2.7 eV) [20,21]. However, it suffers the recombination of charge carriers, the low visible

* Corresponding author at: Graduate Institute of Applied Science and Technology, National Taiwan University of Science and Technology, Keelung Road, Taipei, 10607, Taiwan, ROC.
E-mail address: imae@mail.ntust.edu.tw (T. Imae).

https://doi.org/10.1016/j.jphotochem.2020.112955
Received 20 August 2020; Accepted 25 September 2020
Available online 28 September 2020

light-harvesting ability and hence the low photocatalytic efficiency [22]. Recently it has been reported that when g-CN is hydrothermally introduced oxygen, it makes the product (oxygen-doped g-CN: Og-CN), which is expected to be derived more amount of pores, increased the electron mobility, decreased the charge recombination and enhanced the visible light responsibility [23–26].

In this work, g-CN was synthesized by the thermal condensation polymerization of melamine and followed by the hydrothermal-treating with H_2O_2. The produced oxygen-doped catalyst (Og-CN) was compared to g-CN on their characteristics. The photocatalytic degradation of 2,4-D on the Og-CN catalyst utilizing ultraviolet (UV) and visible light sources was evaluated under the spectrophotometric analysis and compared with that on the g-CN catalyst. The kinetics analysis of the 2,4-D degradation was also performed, and the active species of the reaction was assessed by the trapping experiments. This research will clarify the effective photoreaction activity on Og-CN superior to g-CN and the degradation mechanism of 2,4-D.

2. Experimental

2.1. Reagents and instruments

All chemicals were of analytical grade reagents and used without further purification. Rhodamine 6 G (Rh 6 G), 2,4-dichlorophenoxyacetic acid (2,4-D, 99+ %), melamine powder (99 %), tert-butyl alcohol (99.5 %), potassium iodide, hydrogen peroxide solution (35 wt%) and 2,2,6,6-tetramethyl-1-piperdinyloxy free radical (TEMPO) (98+ %) were purchased from Across Organics (New Jersey, USA). Ultrapure water (resistivity: 18.2 MΩ cm^{-1}) was used throughout this work for the preparation of solutions.

Characterization of materials was done by a Fourier transform infrared (FTIR) absorption spectrophotometer (NICOLET 6700, Thermo Scientific, USA), a UV–vis absorption spectrophotometer (JASCO V-670 and BAS SEC2000, Japan) at a scan speed of 200 nm/min, a transmission electron microscope (TEM, JEOL, JEM-2000FXII, Japan) operating at a 200 kV accelerated voltage, Field-emission scanning electron microscopy (FESEM) JSM 6500 F FE-SEM (JEOL, Tokyo, Japan), and a photoluminescence (PL) spectroscope (F-7000, Hitachi High-Technologies Co., Japan). The X-ray diffraction was recoded on a diffractometer (Bruker, D_2 phaser, Germany) at 5−70° using Cu kα radiation (1.54 Å) at 40 kV and 30 mA, the nitrogen adsorption-desorption isotherm experiment was done at 77 K using a Brunauer-Emmett-Teller (BET) surface area analyzer (BELSORB Max, Japan), the X-ray photoelectron spectroscopic (XPS) measurement was performed on a VG scientific, Model ESCALAB 250, England, a Zahner Zennium Electrochemical workstation (Germany), a Vario TOC select analyzer (Merit Science Corporation, Germany), and the ultrasonic processor (Q700, Misonix, USA) Equipped with a half-inch tip was used for homogenizing.

2.2. Syntheses of photocatalysts

The bulk graphitic carbon nitride was prepared by means of the condensation polymerization of melamine according to the previously reported method [25]. Briefly, melamine powder (7.5 g) was calcined in a ceramic crucible for 4 h at 550 °C in the air atmosphere, and the yellow powder product (bulk graphitic carbon nitride) was collected. The sheet-structured g-CN was prepared by the ultrasonication treatment of the bulk graphitic carbon nitride [27]. Typically, the aqueous dispersion (100 mL) of bulk graphitic carbon nitride (0.2 g) was homogenized for 5 h with an output voltage of 48 W in an ice bath, and the product (g-CN) was filtrated on a 0.2 μm cellulose membrane, washed three times alternately with water and ethanol, and dried overnight at room temperature.

Oxygen-doped graphitic carbon nitride (Og-CN) was synthesized by the solvothermal method [25,28]. Here, g-CN (0.1 g) was dispersed in different percentages of H_2O_2 (10, 20 and 30 %, 60 mL) and stirred for 30 min in water bath at 25 °C, and the dispersion was heated for 4 h at 120 °C in a Teflon-lined stainless autoclave. The solid product was filtrated and washed several times with water.

2.3. Quantum yield and photocatalytic degradation of 2, 4-dichlorophenoxyacetic acid

The fluorescence quantum yields, QY, of two catalysts were calculated by Eq. 1 [29].

$$QY_x = \left(\frac{A_s}{A_x}\right)\left(\frac{F_x}{F_s}\right)\left(\frac{n_x}{n_s}\right)^2 QY_s \quad (1)$$

where A is the absorbance of a UV–vis absorption band, F is an area emission intensity, and n is a refractive index of solvent. Subscripts, s and x, refer to the standard and catalyst. Rhodamine B with a quantum yield of 0.31 was used as a standard.

For the photocatalysis experiment, photocatalyst (g-CN or Og-CN, 15.0 mg, 0.060 mg/mL) was mixed with an aqueous 2,4-D solution (100 ppm, 25.0 mL). An aqueous 2,4-D solution without photocatalyst was also prepared for the blank experiment. The photocatalytic degradation was performed under the UV light irradiation with a 250 W Hg lamp (HOYA-SCHOT EX250 UV light source, JAPAN SERVO Co., Ltd, Japan) or the visible light irradiation (a blue light laser, SEC 2000-DH light source, Japan) at room temperature. The distance of the light source from the surface of the solution was maintained 16 cm for the UV light source, and the visible light source was held at the 1 cm distance to the solution. After the catalyst was dispersed in the analyte solution, the reaction dispersion was constantly stirred for 30 min at the dark condition. When the light was turned on, the reaction time was defined as zero.

The concentration of 2,4-D in a reaction dispersion sampled at the 20 min interval was analyzed using an absorbance of a 283 nm absorption band of 2,4-D and a corresponding calibration curve (Supporting information Fig S1). The absorption spectra of the reaction solutions under the UV light and visible light source irradiations were recorded on a JASCO V-670 spectrophotometer with a 2 mm path length cuvette cell and on a UV–vis spectrometer (SEC 2000, BAS Inc.) with a 10 mm path length cuvette cell, respectively. The total organic carbon (TOC) contents were calculated as % TOC removal by $(TOC_0\text{-}TOC_t)/TOC_0 x100$, where TOC_0 and TOC_t are total organic carbon content before degradation and after degradation at certain time t, respectively. The degradation efficiency was calculated as the degradation ratio or the percent degradation between the initial absorbance of 2,4-D at 283 nm and the corresponding absorbance at a certain reaction time t. For every data, triplicate measurements were averaged. The degradation experiment using the photocatalyst was also applied to Rh6 G dye for comparison.

For active species-trapping (scavenging) experiments, trapping reagent (TEMPO, KI, or t-BuOH, 10 mM, 1 mL) was added to an aqueous 2,4-D solution and the photodegradation experiments were performed.

2.4. Optical properties of the materials

In order to estimate the bandgap of the materials, a Tauc's Eq. 2 was used.

$$\alpha h\upsilon = c\,(h\upsilon - Eg)^{n} \quad (2)$$

where Eg is a bandgap energy, α is an absorption coefficient, hυ is an energy absorbed, and c and n are constants. In order to calculate the flat band potential, which is assumed to be the energy of the conduction band (E_{CB}) with respect to the energy of normal hydrogen electrode (NHE), a Mott-Schottky equation (Eq. 3) was applied by extrapolating the linear portion of the plot to the x- axis [30].

$$\frac{1}{C^2} = \left(\frac{2}{\varepsilon\varepsilon_0 A^2 eND}\right)\left[V - \left(V_{fb} + \frac{KT}{e}\right)\right] \quad (3)$$

Where C, ε, ε_0, A, e, ND, V, V_{fb}, K, and T are the capacitance at the space charge region, the dielectric constant of the semiconductor, the permittivity of free space, the donor density (electron donor concentration for an n-type or hole acceptor concentration for p-type semiconductors), the applied potential, the flat band potential, the Boltzmann constant, and the temperature, respectively [30,31]. Then, Eg and E_{CB} ($\equiv V_{fb}$) are obtained from the plots of $\alpha h\upsilon$ vs $h\upsilon$ and C^{-2} vs V plots, respectively.

3. Results and discussion

3.1. Characterization of photocatalysts

To assess the photocatalytic activities, the photocatalysts (g-CN and Og-CNs) were synthesized and characterized. As indicated in the TEM images (Fig. 1), both catalysts (g-CN and 2-Og-CN) represented the morphology where the sheet-like textures with amorphous shape are agglomerated. Similar TEM images of g-CN and 2-Og-CN have been reported [31]. The surface morphologies of pristine g-CN and oxidized 2-Og-CN were also visualized via FE-SEM. As depicted in Fig. 1B(a,b), the sheet like structures of the materials were observed. The elemental compositions of carbon, nitrogen, and oxygen of g-CN and 2-Og-CN were determined from energy dispersive X-ray spectroscopy (EDS) analysis as shown in Fig. 1C(a,b). After the hydrothermal treatment of g-CN, the increment of oxygen (1.5%–6.8%) along with the decrease in atomic percentage of nitrogen (63.6–56.2%) indicates that some nitrogen atoms were replaced by oxygen atoms.

Then thermal heating of melamine molecules can produce the covalent organic framework consisting of heptazine unit as illustrated in Scheme 1, which was confirmed from N/C ratio > 1.5 obtained from EDS analysis [32]. The hydrothermal oxidation of g-CN generates the oxidized g-CN (Og-CN), where some nitrogen atoms in amine (C-NH_x (x = 1 or 2), C = N-C or N-C_3 bonds) will be replaced by oxygen to produce C—OH or C—O—C bonds (see Scheme 1) [31,33].

The FTIR absorption spectra of g-CN and Og-CNs are shown in Fig. 2A,B. A broad absorption band centered around 3300−3100 cm^{-1} indicates the existence of an N—H stretching vibration band resulting from amine groups. Several bands at 1650−1200 cm^{-1} correspond to the stretching modes of heterocyclic C—N bonds. Specifically, 1640, 1410, 1322 and 1250 cm^{-1} bands are attributed to C═N, C—N, N-C_3 and NH-C_2 stretching vibration modes, respectively, of heptazine unit. A band at 810 cm^{-1} is referred to the breathing mode (out of plane bending vibration mode) of heptazine units [34]. Additionally, after

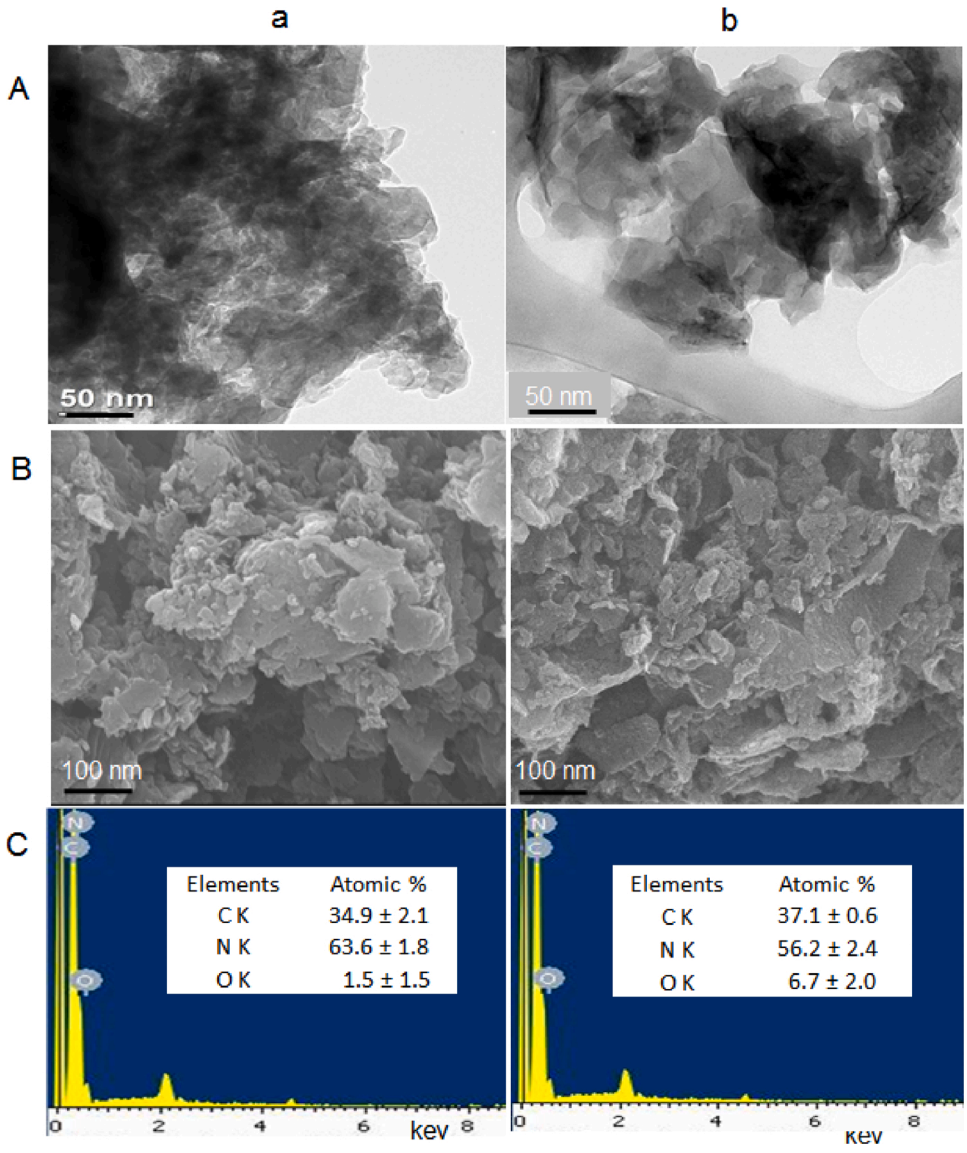

Fig. 1. (A) HRTEM images, (B) FE-SEM images and (C) EDS analysis with inset atomic mass percentages of (a) g-CN and (b) 2-OgCN.

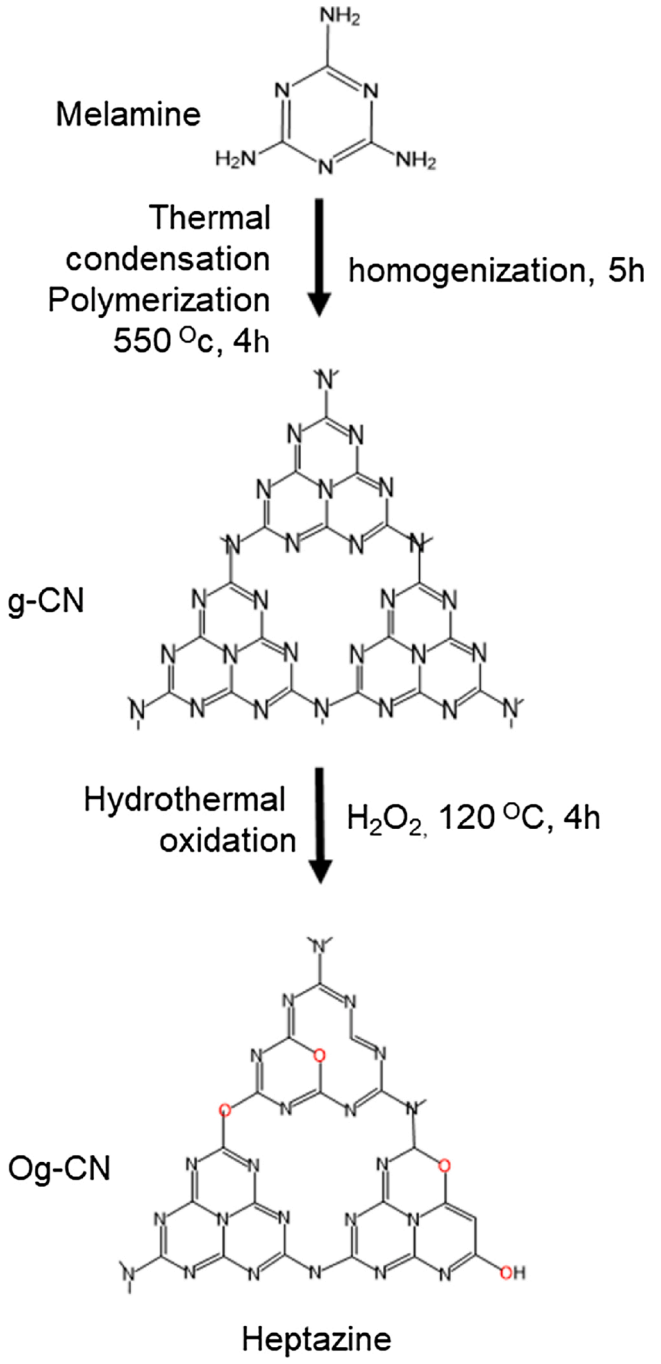

Scheme 1. Schematic illustration of reaction processes and their products on photocatalyst (g-CN and Og-CN) syntheses.

treating g-CN with different concentrations of H_2O_2, a new peak at 1208 cm^{-1} appeared (Fig. 2B), corresponding to the C-O-C stretching vibration mode [35], although C—OH bands were not clarified because of the less or overlapped contribution. Thus, IR spectra confirmed the existence of heptazine units in both semiconductors and oxidized units in the oxidized materials [35].

As seen in the UV–vis absorption spectra of g-CN and Og-CNs shown in Fig. 2C, the strong absorption band of g-CN was observed at 330 nm following shoulders around 230 and 400 nm, and a similar spectrum was observed even for Og-CNs. The influence of oxidation on the electronic property of g-CN was rather clarified on the PL spectra, where an emission band at 440 nm with a shoulder band around 460 nm was measured at the 275 nm excitation for both photocatalysts, as seen in Fig. 2D. Although the additional excitation bands were observed at 330, and 360 nm, the emission spectra at the 330 nm and 360 nm excitation generated relatively lower emission intensities at 440 nm, indicating that the main excitation band is at 275 nm. It should be noticed that the PL emission intensities of g-CN decreased after the oxidation, because the more electronegative oxygen atom effectively suppresses the recombination of the photo-generated electron-hole carriers (e^-/h^+) [31]. Additionally, there was a small red shift of an emission band as observed. This band shift is attributed to change in electronic structure after much doping the electronegative oxygen. The quantum yields of two catalysts were calculated by using Rhodamine B as a reference and obtained 14.8 % and 13.9 % for g-CN and 2-Og-CN, respectively, and those values are comparable with the reported values (12.5 %, 10.3 %) for graphitic carbon nitride-type semiconductors [36,37].

The XPS survey spectra, the XPS fine spectra with deconvolution and the lists of deconvoluted species of precursor (melamine) and two catalysts (g-CN and 2-Og-CN) are shown in Fig. 3 and Table 1. As seen in Fig. 3Aa, Ba and Ca, the former two compounds (melamine and g-CN) mainly consist of carbon and nitrogen elements but the intensity of oxygen element in 2-Og-CN increased because Og-CN is a product of oxidation reaction of g-CN. The deconvolution analysis of high-resolution C 1s and N 1s spectra of melamine (Fig. 3Ab and 3Ac) displayed each two distinguishable peaks with binding energies at 285.7 and 288.9 eV (C 1s) and at 398.4 and 399.6 eV (N 1s). Based on these binding energies, the structural change was examined for the other two materials after polymerization and oxidation. The deconvoluted C 1s and N 1s spectra of g-CN (Fig. 3Bb and Bc) revealed additional peaks besides melamine-based bonds (C-NHx(x=1,2) and C=N-C). There are C 1s peaks at 283.1 and N 1s peak at 400.2 eV which was attributed to N-C_3 in heptazine and additionally C 1s peaks at 287.2 eV corresponds to NH$\underline{C}O_2$/$\underline{C}$OH appeared for g-CN [38–42]. On 2-OgCN, although the same numbers of C 1s and N 1s peaks as those on g-CN were deconvoluted, the relative strengths of C 1s peaks varied: Melamine-based C 1s peaks became weaker and alternatively a new peak at 284.4 eV appeared (Fig. 3Cb). This variation can be attributed to the oxidation of C-NHx(x = 1,2), C = N-C or N-C_3 bond to C—O—C/COH bond [34–36]. The oxidation also influenced the N 1s peaks (Fig. 3Cc). Among three N 1s peaks of g-CN, the area intensity of a 398.1 eV peak especially decreased after the oxidation. Correspondingly, the O 1s spectrum of 2-Og-CN presented the $\underline{C}$-O-C/COH peaks at 530.3 and 531.6 eV (Fig. 3Cd) [42]. Thus, it was proved from the analysis of XPS that the heptazine unit exists in g-CN and the oxidation of g-CN produces some oxidized COC/COH bonds as illustrated in Scheme 1.

The XRD patterns of g-CN, 1-Og-CN, 2-Og-CN and, 3-Og-CN are shown in Fig. 4A. The main peak at $2\theta = 27.95°$ in g-CN is reported as a (002) plane of the lamellar structure and this plane can be attributed to the interplane distance of the stacked heptazine structures [40]. The d-spacing of this peak was evaluated to be 0.318 nm, and this peak showed the angle shift to $2\theta = 28.03°$ or the d-spacing shift to 0.317 nm in Og-CN. Since this shift is negligibly small, it can be interpreted that the oxidation scarcely affected the interplane distance. The second peak observed at $2\theta = 13.45°$ corresponding to the d-spacing of 0.663 nm is associated with (100) plane, but also assigned to be the (210) reflection of orthorhombic structure [43]. In any case, this peak angle of Og-CN did not vary from it of g-CN, indicating no in-plane structural variation between them. Thus, the XRD result confirmed that the crystal structure of g-CN was not influenced by the oxidation. The peaks of g-CN around 2Θ (35–40) can be assigned to uncondensed melamine structure, which may be fully condensed after hydrothermal treatment [44,45].

As indicated in Fig. 4B, the nitrogen adsorption-desorption curves of g-CN, 1-Og-CN, 2-Og-CN and, 3-Og-CN belong to the type IV isotherm with a hysteresis at high relative pressure, which indicates the mesoporous structure of these catalysts. The specific surface area, pore volume, and pore diameter of the catalysts were evaluated from these isotherms and Barrett, Joyner and Halenda (BJH) plots. The Og-CN(s) exhibited slightly larger specific surface area and pore volume, and

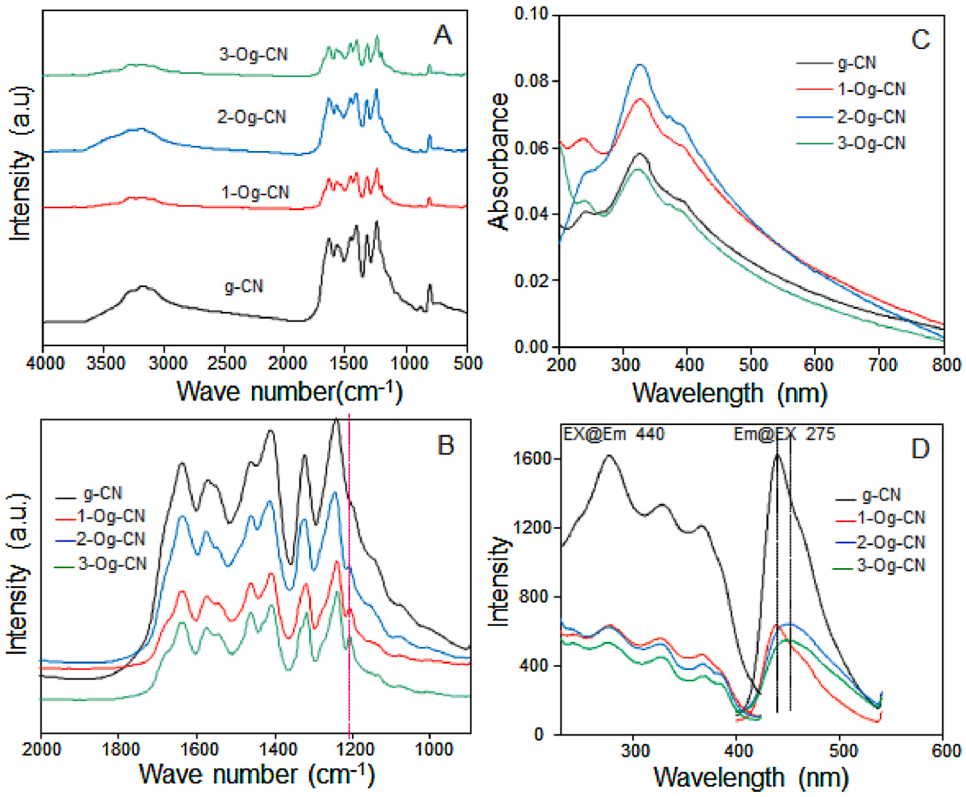

Fig. 2. (A) (B) FTIR absorption spectra (C) UV–vis absorption spectra and (D) PL spectra of g-CN and Og-CNs.

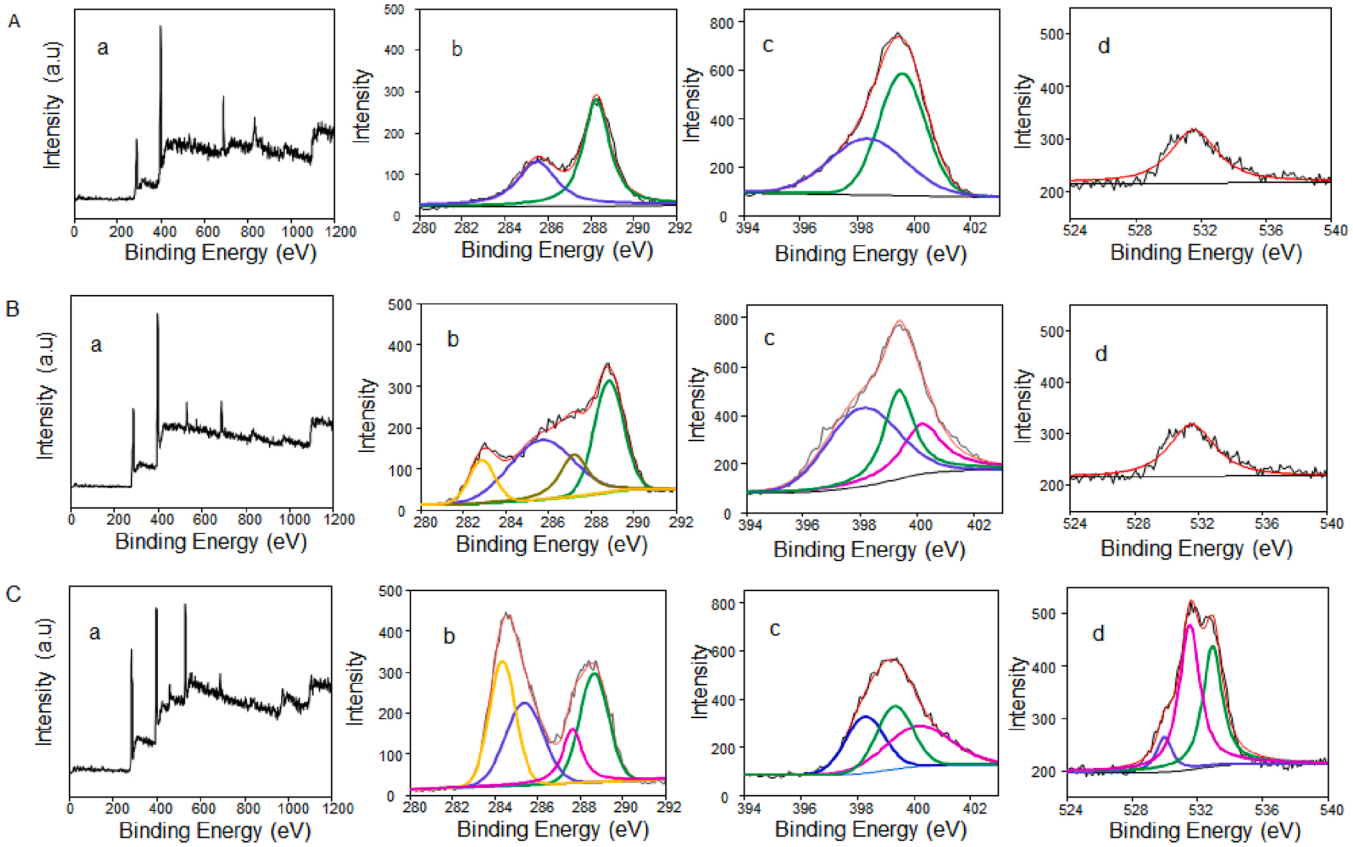

Fig. 3. (a) Survey XPS spectra of (A) melamine, (B) g-CN and (C) 2-Og-CN and their high resolution XPS spectra and deconvoluted peaks of (b) C 1s, (c) N 1s and (d) O 1s.

Table 1
XPS deconvoluted peaks and their assignments for g-CN and 2-OgCN [34,35,39–42].

Element	Melamine		g-CN		2-Og-CN		Assignment*
	BE (eV)	Area intensity (a.u.)	BE (eV)	Area intensity (a.u.)	BE (eV)	Area intensity (a.u.)	
C 1 s			283.1	166.5	284.4	470.9	$^{b,c}CN_3$
	285.5	344.5	285.7	554.7	285.5	444.3	^{a,b,c}C-NHx(x = 1,2)
			287.2	236.9	287.7	241.6	$^{b,c}NHCO_2^-$/^{c}C-O-C/COH
	288.3	546.9	288.9	467.3	288.7	446.0	^{a,b,c}C=N-C
N 1 s	398.4	798.4	398.1	988.1	398.1	287.6	^{a,b,c}C-NHx(x = 1,2)
	399.6	1030.1	399.4	654.9	399.4	575.8	^{a,b,c}C=N-C
			400.2	537.2	400.2	415.2	$^{b,c}NC_3$
O 1 s					530.3	108.4	^{c}C-O-C/OH
					531.6	614.3	^{c}C-O-C/OH
	532.5	329.6	532.3	501.5	532.9	466.4	$^{a,b,c}NHCO_2^-$

* Assignment to [a]melamine, [b]g-CN, and [c]2-OgCN.

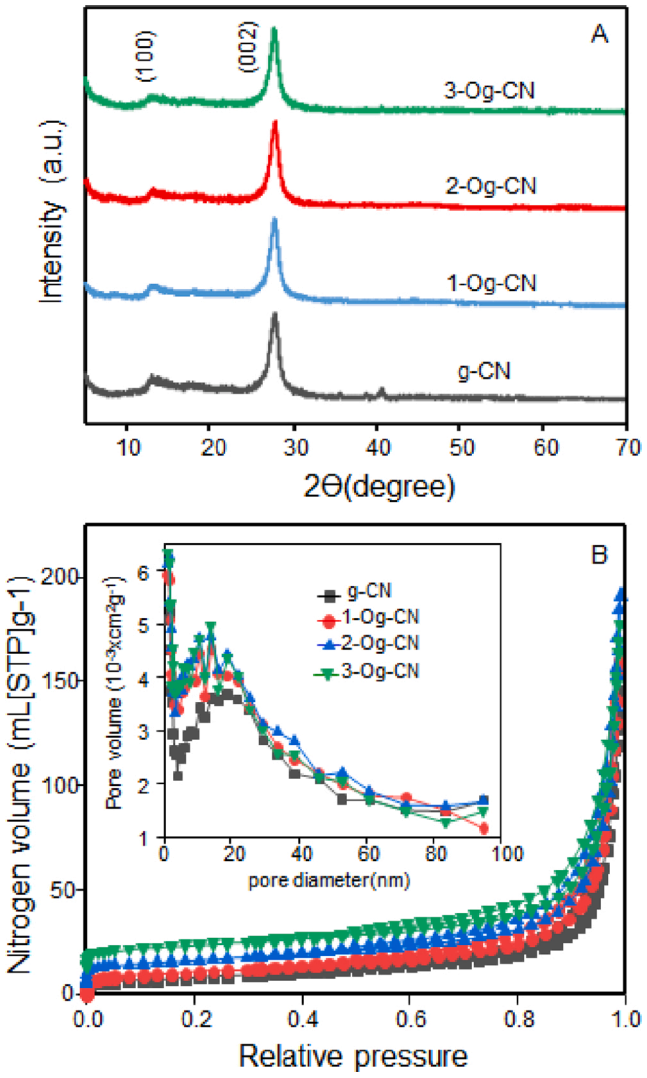

Fig. 4. (A) XRD patterns and (B) nitrogen adsorption-desorption isotherms of g-CN and Og-CNs. Inset in (B) is their BJH pore-size distributions.

lesser pore diameter than g-CN as shown in Table 2. The results of nitrogen adsorption-desorption isotherms showed the increase in surface area and porosity (pore volume) with increase in oxygen content, although pore diameter decreased with oxygen content (Table 2 and Fig. 4 inset). The decrease of pore volume at highest oxygen content (3-Og-CN) as well as similarity of its surface area to 2-Og-CN may relate to the limitation of the oxygen content on photocatalytic activity as

Table 2
Analyses of nitrogen adsorption-desorption isotherms.

catalyst	specific surface area ($m^2 g^{-1}$)	pore volume ($cm^2 g^{-1}$)	pore diameter (nm)
g-CN	28.35	0.224	31.63
1-Og-CN	37.22	0.242	26.53
2-Og-CN	39.32	0.262	26.68
3-Og-CN	40.02	0.247	24.73

described above. Thus, increase in oxygen content increases the porosity and specific surface areas of the materials up to certain maximum limit. The values of the surface area obtained was comparable to the previously reported values for graphitic carbon nitride-type semiconductors [29]

It was confirmed from the characterizations described above that g-CN and Og-CNs were constructed from heptazine unit, and the oxidation of g-CN changed C—N=C group to ester group or terminal amine group to hydroxyl group. According to this chemical modification, Og-CNs lowered the quantum yield of PL emission and increased the surface area. These variations should influence the catalytic properties.

3.2. Photocatalytic degradation of 2,4-D by g-CN and Og-CN

The herbicide 2,4-D has two absorption bands at 230 and 283 nm, which correspond to the $\pi - \pi^*$ and $n - \pi^*$ transitions, respectively, as seen in (Supporting information Fig S1). Photocatalytic degradation of 2,4-D by g-CN and 2-Og-CN was performed under the UV and visible light irradiations. Then the absorption spectra of 2,4-D at 283 nm decreased with the reaction time as seen in Figs. 5Aa,b, Ba,b and S2. The % degradation of 2,4-D by different catalysts under UV and visible light irradiations was plotted in Fig. 5Ac,Bc, which was calculated using the absorbance at 283 nm and also included the result of the degradation reaction of 2,4-D without catalyst under UV light irradiation. It should be noted that the slight degradation (about 20 % at 140 min irradiation) happened even without catalyst. This slight degradation can be explained by the absorption of energy from the UV light source, which produces the excited state (2,4-D*), leads the excited singlet state (^{1}2,4-D) and gives rise to the triplet state (^{3}2,4-D) through the non-radiative transition [46].

The photocatalytic degradation of 2.4-D increased from g-CN and 1-Og-CN to 2-Og-CN but that of 3-Og-CN was almost similar to that of 2-Og-CN. As a result, 2-Og-CN was focused and analyzed in comparison to g-CN. As seen in Fig. 5Ac,Bc, the degradation of 2,4-D was accelerated in the presence of catalysts g-CN and 2-Og-CN under the photo irradiation and reached a maximum of 96.3 % and 98.7 % after 140 min under the UV light irradiation and 21.8 % and 61.5 % after 120 min under the visible light irradiation, respectively. The results indicate that the UV

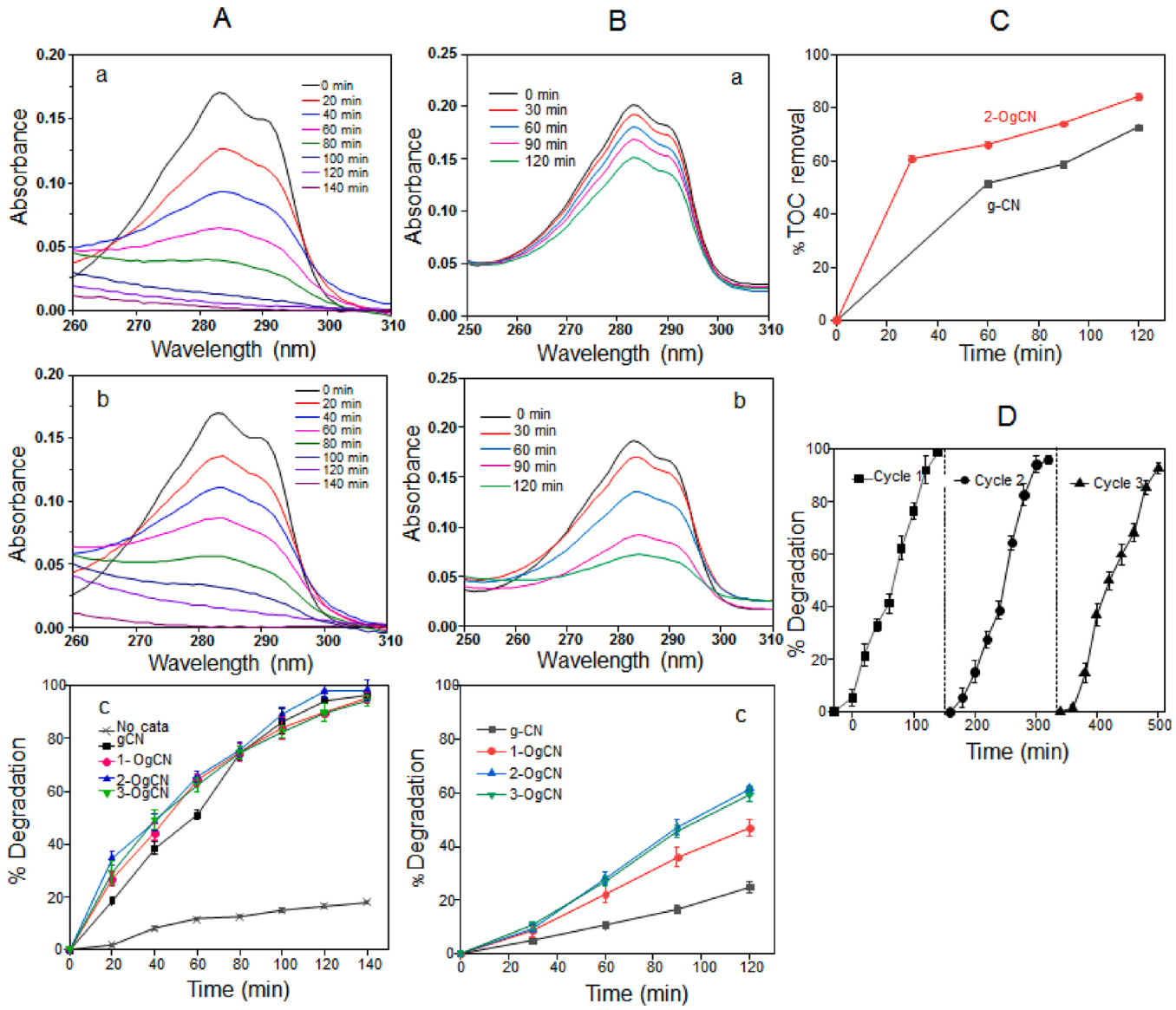

Fig. 5. UV–vis absorption spectra of 2,4-D on photocatalytic degradation reaction process under (A) UV and (B) visible light irradiations by (a) catalyst g-CN and (b) catalyst 2-Og-CN. (c) The % degradation of 2,4-D as a function of reaction time for no catalyst, g-CN, 1-Og-CN, 2-Og-CN and 3-Og-CN under (A) UV and (B) visible light irradiations. (C) The % TOC removal after the degradation reaction of 2,4-D by g-CN and 2-Og-CN catalysts under UV light Source. (D) Recyclability examination by three successive degradations of 2,4-D on catalyst 2-Og-CN under UV light irradiation.

light source is remarkably effective superior to the visible light source and Og-CN is more active as a photocatalyst than g-CN.

TOC was selected as the mineralization index for the degradation products of 2,4-D and the time dependent TOC removal from 2,4-D solutions during the photoreaction under UV light source was displayed in Fig. 5C. The TOC removal rate reached highest percentage of 84.2 % at 120 min for 2-Og-CN catalyst but it for g-CN was 72.5 % at 120 min. These numerical values indicate that 77 and 88 % of degraded 2,4-D by g-CN and 2-Og-CN, respectively, were decomposed to become CO_2 and H_2O, as the photodegradation of 2.4-D was 94.5 and 95.6 % by g-CN and 2-Og-CN, respectively, after 120 min UV light irradiation. Thus, the 2-Og-CN catalyst is high in TOC removal rate compared to the g-CN catalyst and the catalysts have sufficiently better degree of mineralization for practical uses [47,48].

The recyclability is the prerequisite for the catalysts to be used in the practical application. As shown in Fig. 5D, the reusability was tested by using catalyst 2-Og-CN for three successive 2,4-D degradations under the UV light irradiation and over 94 % of the original photocatalytic activity was retained, indicating the excellent photocatalytic recyclability of the 2-Og-CN. This decrease may be due to the photocorrosion [41].

3.3. Photocatalytic degradation kinetics

To analyze the kinetics of photocatalytic degradation of organic pollutants, the conventional Langmuir-Hinshelwood (L-H) model can be used, as indicated in Eq. 4 [49].

$$\frac{-dC}{dt} = \frac{kKC}{1 + KC} \tag{4}$$

where C is the concentration of pollutant at a reaction time t and k and K are the photo-degradation rate constant and the adsorption constant, respectively. These equations can be simplified under some conditions. For KC>>1, Eq. 4 becomes Eq. 5 and can be expressed as Eq. 6 when integrated under the boundary condition of the initial concentration, C_0, to the concentration, C_t, at the degradation time t. Then Eq. 6 is the

zeroth order kinetics equation.

$$-dC/dt = k \quad (5)$$

$$C_t - C_0 = -kt \text{ or } \frac{C_t}{C_0} = -\frac{k}{C_0}t + 1 \quad (6)$$

When $KC << 1$, Eq. 4 can be reduced to give an Eq. 7 and the integrated Eq. 8, which is the first order reaction.

$$-dC/dt = kKC \quad (7)$$

$$\ln(C_t/C_0) = -kKt \quad (8)$$

Based on the theoretical Equations described above, the % degradation vs time plot of selected catalysts (g-CN and 2-Og-CN) under both light sources in Fig. 5Ac,Bc was replotted to be the C_t/C_0 vs time plot. As seen in Fig. 6, the fitting or the linearity to the zeroth order type reaction equation was good. The degradation rate constant k and the variance R^2 values for different light sources and different catalysts are listed in Table 3 and the kinetics fittings are indicated in Fig. 6. The kinetics rate constants follow the order of 2-Og-CN (UV) > g-CN (UV) > 2-Og-CN (Vis) > g-CN (Vis) ≈ no catalyst (UV) and the variances were always higher than 0.99. Separately, $\ln(C_t/C_0)$ values were plotted as a function of reaction time following the first order Eq. 6. As seen in Fig S3 and Table S1, although the linearity of $\ln(C_t/C_0)$ against reaction time was found, the variance of the fitting linearity dissipated from 0.92 to 0.99 and was inferior to the fitting based on the zeroth order type reaction equation. Thus, it can be noted that the catalytic performance of 2-Og-CN was higher than that of g-CN, the UV light was more preferable than the visible light as an irradiation light source, and the reaction follows to the zeroth order kinetics equation.

Table 4 summarizes the degradation reports of 2,4-D using different catalysts [8,14,50–53]. Most of the previous reports were performed using metal oxide photocatalysts like TiO_2 and ZnO except the $ZnIn_2S_4$/g-CN catalyst [49]. Although the present experiments confirmed that the irradiation of UV lamp is more effective than that of visible light and the other researches were also examined on UV light, the visible light also acted well on MoO_3/ZnO nanorod catalyst [54]. When the percent degradation and the reaction time were compared in association with the light intensity, catalyst dosage, and initial concentration of 2,4-D, it can be noted that even for highly degrading metal-based catalysts (MoO_3/ZnO nanorod (99 %) and hydrothermal TiO_2 (96 %)) [50,52], the amount of the catalyst used was large in comparison with the present works. Additionally, with respect to %TOC

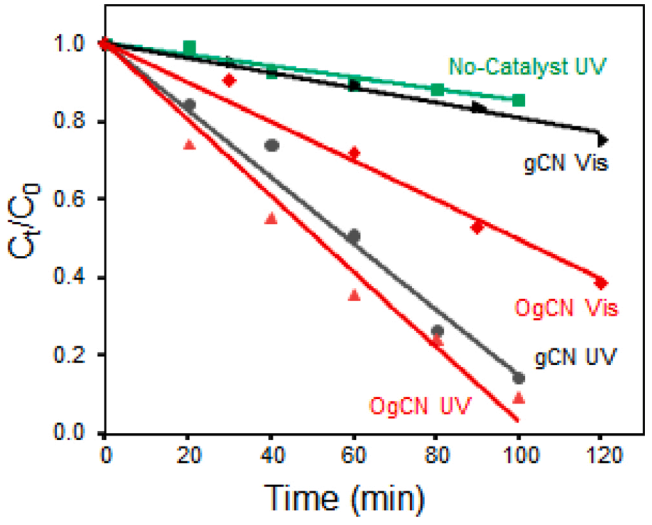

Fig. 6. C_t/C_o plots of 2,4-D as a function of time for no catalyst under UV light irradiation and g-CN and 2-Og-CN under UV and visible light irradiations.

Table 3
Kinetics data obtained from the fitting to the zeroth order equation.

Variable	No catalyst, UV	g-CN, Vis	2-Og-CN, Vis	g-CN, UV	2-Og-CN,. UV
k (ppm/min)	0.00150	0.00194	0.00503	0.00854	0.00975
R^2	0.99977	0.99983	0.99808	0.99518	0.99025

removal the present catalysts g-CN and 2-Og-CN reached 72.5 % and 84.2 % respectively within 120 min and shows remarkably superior performance compared to reports in the Table. Besides, even if the initial concentration of 2,4-D was large in the present case, the reaction was accomplished at the similar time as the other reports. As a result, the present metal-free covalent-organic framework photocatalysts (g-CN and Og-CN) reacted similarly as or more effectively than inorganic metal-oxide-based photocatalysts.

The catalytic quality of two catalysts was evaluated even on the degradation of Rh 6 G dye. The excellent photo-degradation capacity of the two catalysts was also proved on the degradation of Rh 6 G dye: The dye was almost completely degraded within 20 min under the UV light irradiation (Fig S4). The result also showed the higher catalytic performance over the metal oxide-based catalysts because of a higher rate of degradation of Rh 6 G at the higher initial dye concentration by g-CN and Og-CN [55].

3.4. Mechanisms of photocatalytic reaction

In order to confirm the active species involved in the photocatalytic reaction, the active species-trapping experiment was performed. The photodegradation of organic substances assisted by photon-irradiated semiconductors results in the generation of electron/hole (e^-/h^+) pair, which may produce hydroxyl radical ($^{\bullet}OH$) and/or superoxide radical anion ($O_2^{\bullet-}$) capable to react with the active sites [52,53]. Therefore, the mechanism of photocatalytic degradation of 2,4-D can be interpreted based on the trapping process of active species. This examination was done by introducing TEMPO, t-BuOH and KI as effective scavengers for $O_2^{\bullet-}$, $^{\bullet}OH$, and h^+, respectively, during the photodegradation [48]. As indicated in Fig. 7A, when the photodegradation of 2,4-D by 2-Og-CN under the UV light irradiation was performed in the presence of scavengers, all scavengers had a suppression effect on the degradation reaction of 2,4-D, and the degree of suppression decreased in the order of TEMPO > t-BuOH > KI. This result indicates that $O_2^{\bullet-}$ was more active and followed by ·OH and h^+ in the participation of reaction. Thus, the effective scavengers scavenge active species generated from the photocatalysts and suppress the reaction of active species with 2,4-D. Then the proposed reaction mechanism by the active species and the final reaction products are indicated below, as described in Eqs. 9–12.

A plausible mechanism for the photocatalytic activities with respect to band gap and the separation of photo-generated electron-hole pairs was also proposed. The conduction band (CB) and valence band (VB) potentials was calculated from flat band of the Mott-Schottky plot (Fig. 7B), which is the x intercept of the linear portion for g-CN and 2-Og-CN were -0.72 and -0.78 eV vs NHE respectively as indicated in Fig. 7A. Similarly, the Eg values for selected 2-Og-CN is 2.70 and that of g-CN is 2.89 calculated from Tacu's plot (Fig. 7C). Based on the calculated Eg, ECB, and EVB the mechanistic diagram was indicated with respect to the redox potentials of the materials verses the NHE as indicated in Fig. 7D. Then the reaction mechanism can be illustrated in Fig. 7E.

$$\text{Semiconductor (photocatalyst)} + h\nu \rightarrow e^-(\text{Og-CN, CB}) + h^+(\text{Og-CN, VB}) \quad (9)$$

$$Og - CN + H_2O(\text{adsorbed}) \rightarrow Og - CN + OH^- + {}^{\bullet}OH \quad (10)$$

$$e^-(Og - CN, CB) + O_2 \rightarrow Og - CN + O_2^{\bullet-} \quad (11)$$

Table 4
Comparison of the catalytic degradation of 2,4-D.

Catalyst	Light Source	Catalyst Dosage (mg/mL)	2,4-D Dosage (ppm)	Reaction Time (min)	% Degradation	%TOC removal	Reference
Nitrogen-doped TiO_2	Visible light, 250 W	0.1(mg)	40	180	83	ND	[50]
Hydrothermal TiO_2	UV lamp, 11 W	0.2	50	120	96	44	[52]
Pt/TiO_2	Mercury lamp, 400 W, 365 nm	0.12	20	90	≥90	ND	[53]
Fe@ZrO_2	UV lamp, 254 nm	1	50	150	60		[14]
MoO_3/ZnO nanorod	Visible light	1.5	20	120	99	23	[54]
Tourmaline-coated TiO_2	UV lamp, 200–1000 W/m, 254 nm	0.5	20	40	>90	ND	[8]
$ZnIn_2S_4$/g-CN	Xe lamp, 500 W	0.02	100	180	90	41.6	[49]
gCN	Visible light	0.06		120	21	ND	Present Work
OgCN	Visible light	0.06	100	120	61	ND	Present Work
gCN	UV lamp, 4.5 W	0.06	100	140	97	72.5 (120 min)	Present Work
OgCN	UV lamp, 4.5 W	0.06	100	140	99	84.2 (120 min)	Present Work

ND: not detected.

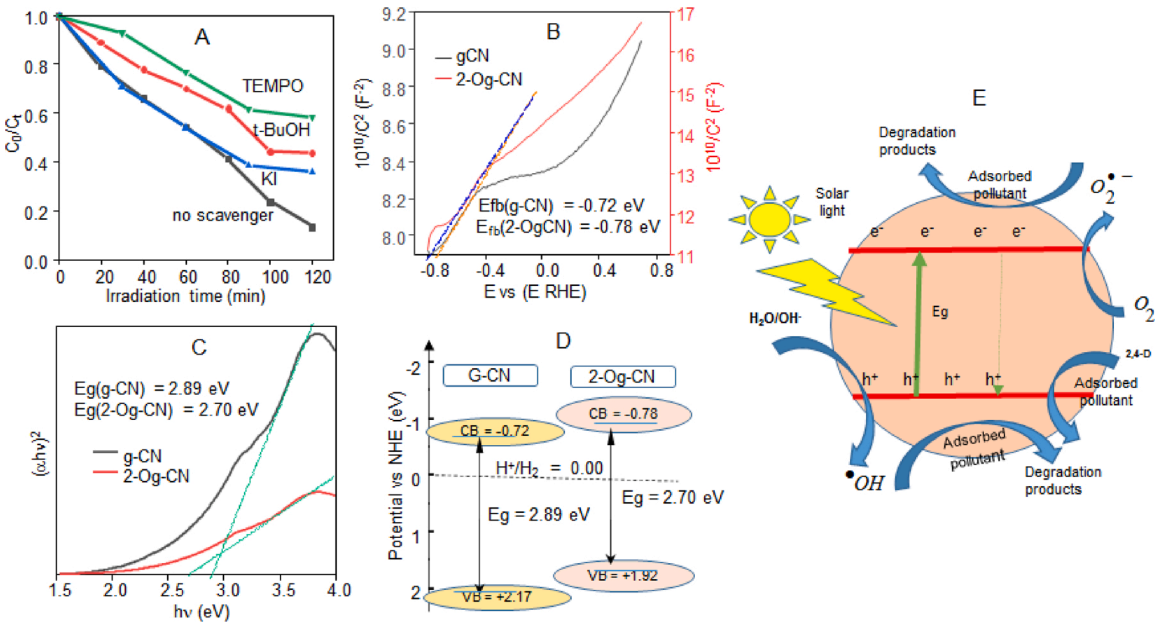

Fig. 7. (A) The effects of scavengers (t-BuOH, TEMPO and KI) on the degradation of 2,4-D by 2-Og-CN under UV visible light irradiation, (B) Mott-Schottky plots of g-CN and 2-Og-CN, (C) Tauc's plots of g-CN and 2-Og-CN, (D) the band energy diagram with respect to NHE, and (E) the schematic illustration of the photodegradation on a catalyst Og-CN.

$$2,4-\mathrm{D}\left(O_2^{\bullet-}, {\bullet}OH \text{ or } h^+\right) \rightarrow \text{Degradation product} \quad (12)$$

It was revealed that the higher degradation was observed on the UV light irradiation as compared to the visible light irradiation. This is ascribed to the higher threshold energy of UV ray as compared to the visible light source of the lower energy. The electronegative oxygen atom in Og-CN can effectively suppress the recombination of photogenerated electrons and holes which can also enhance the photocatalytic efficacy.

4. Conclusions

In this work, the photocatalytic degradation performance of Og-CN on 2,4-D pesticide with UV and visible light sources was reported and compared with that of g-CN. Because some amounts of oxygen were displaced the nitrogen atom in the g-CN, the surface area and PL properties of Og-CN varied from those of g-CN, and the photocatalytic degradation efficiency of 2,4-D increased compared to the g-CN catalysts. The superoxide ion ($O_2^{\bullet-}$) species, which dominates in photocatalytic degradation of 2,4-D, should be generated more from oxidized material (Og-CN), and thus Og-CN becomes more effective on the photocatalytic performance than that of g-CN. The increment in the photocatalytic activity of Og-CN should also be attributed to the increase in electron mobility of elemental oxygen and the decrease in recombination rate, which can be improved after oxidation. As a result, Og-CN exerted the photocatalytic activity and, especially, its total organic carbon removal was remarkably high different from inorganic catalysts.

Because g-CN-based materials are metal-free, low toxic, and synthesized from most abundant materials, they are prospective photocatalysts as well as the semiconductor material. However, their low visible light responsiveness hinders its catalytic ability in visible light. Thus, to use g-CN-based materials as metal-free photocatalysts for reactions and to be applied as semiconductors for energy generation and storage, the demanding more research is requested in the improvement of the bandgap by hybridizing or doping other semiconductor materials.

Declaration of Competing Interest

The authors report no declarations of interest.

Acknowledgments

This investigation was partly supported by the Ministry of Science and Technology, Taiwan (MOST 107-2221-E-011-067-). S.Y.E. fully acknowledges and appreciates the National Taiwan University of Science and Technology, Taiwan, for the opportunity of studying and the financial support of PhD student scholarship. We give thanks to Prof. Lai and Prof. Hu in the National Taiwan University of Science and Technology, Taiwan, for their kind measuring of TOC.

Appendix A. Supplementary data

Supplementary material related to this article can be found, in the online version, at doi:https://doi.org/10.1016/j.jphotochem.2020.112955.

References

[1] D.A. Alvarez, W.L. Cranor, S.D. Perkins, R.C. Clark, S.B. Smith, Chemical and toxicologic assessment of organic contaminants in surface water using passive samplers, J. Environ. Qual. 37 (2008) 1024–1033.
[2] S. Stehle, R. Schulz, Agricultural insecticides threaten surface waters at the global scale, Proc. Natl. Acad. Sci. U. S. A. 112 (2015) 5750–5755.
[3] J.C.G. Sousa, A.R. Ribeiro, M.O. Barbosa, M.F.R. Pereira, A.M.T. Silva, A review on environmental monitoring of water organic pollutants identified by EU guidelines, J. Hazard. Mater. 344 (2018) 146–162.
[4] F.A. Chinalia, M.H. Regali-Seleghin, E.M. Correa, 2, 4-D toxicity: cause, effect and control, Aquatic. Environ. Toxicol. 1 (2007) 24–33.
[5] K.H. Kim, E. Kabir, S.A. Jahan, Exposure to pesticides and the associated human health effects, Sci. Total Environ. 575 (2017) 525–535.
[6] B. Ismail, M. Sameni, M. Halimah, Evaluation of herbicide pollution in the kerian ricefields of Perak, Malaysia, World Appl. Sci. J. 15 (2011) 05–13.
[7] F. Islam, J. Wang, M.A. Farooq, M.S.S. Khan, L. Xu, J. Zhu, M. Zhao, S. Munos, Q. X. Li, W. Zhou, Potential impact of the herbicide 2,4-dichlorophenoxyacetic acid on human and ecosystems, Environ. Int. 111 (2018) 332–351.
[8] X. Bian, J. Chen, R. Ji, Degradation of 2,4-dichlorophenoxyacetic acid (2,4-D) by novel photocatalytic material of tourmaline-coated $TiO_{(2)}$ nanoparticles: kinetic study and model, Materials (Basel) 6 (2013) 1530–1542.
[9] L. Tang, S. Zhang, G.M. Zeng, Y. Zhang, G.D. Yang, J. Chen, J.J. Wang, J.J. Wang, Y.Y. Zhou, Y.C. Deng, Rapid adsorption of 2,4-dichlorophenoxyacetic acid by iron oxide nanoparticles-doped carboxylic ordered mesoporous carbon, J. Colloid Interface Sci. 445 (2015) 1–8.
[10] L. Ding, X. Lu, H. Deng, X. Zhang, Adsorptive removal of 2,4-Dichlorophenoxy-acetic acid (2,4-D) from aqueous solutions using MIEX resin, Ind. Eng. Chem. Res. 51 (2012) 11226–11235.
[11] E.E. Ebrahiem, M.N. Al-Maghrabi, A.R. Mobarki, Removal of organic pollutants from industrial wastewater by applying photo-Fenton oxidation technology, Arab. J. Chem. 10 (2017) S1674–S1679.
[12] S.P. Kamble, S.P. Deosarkar, S.B. Sawant, J.A. Moulijn, V.G. Pangarkar, Photocatalytic degradation of 2, 4-dichlorophenoxyacetic acid using concentrated solar radiation: batch and continuous operation, Ind. Eng. Chem. Res. 43 (2004) 8178–8187.
[13] Y. Nakanishi, T. Imae, Synthesis of dendrimer-protected TiO_2 nanoparticles and photodegradation of organic molecules in an aqueous nanoparticle suspension, J. Colloid Interface Sci. 285 (2005) 158–162.
[14] S. Kundu, A. Pal, A.K. Dikshit, UV induced degradation of herbicide 2,4-D: kinetics, mechanism and effect of various conditions on the degradation, Sep. Purif. Technol. 44 (2005) 121–129.
[15] M. Alvarez, T. López, J.A. Odriozola, M.A. Centeno, M.I. Domínguez, M. Montes, P. Quintana, D.H. Aguilar, R.D. González, 2,4-Dichlorophenoxyacetic acid (2,4-D) photodegradation using an Mn^{+}/ZrO_2 photocatalyst: XPS, UV–vis, XRD characterization, Appl.Catal B: Environ. 73 (2007) 34–41.
[16] G. Dong, Y. Zhang, Q. Pan, J. Qiu, A fantastic graphitic carbon nitride ($g\text{-}C_3N_4$) material: electronic structure, photocatalytic and photoelectronic properties, J. Photochem. Photobiol. C Photochem. Rev. 20 (2014) 33–50.
[17] J. Liu, H. Wang, M. Antonietti, Graphitic carbon nitride "reloaded": emerging applications beyond (photo) catalysis, Chem. Soc. Rev. 45 (2016) 2308–2326.
[18] Z. Zhao, Y. Sun, F. Dong, Graphitic carbon nitride based nanocomposites: a review, Nanoscale 7 (2015) 15–37.
[19] S. Kang, W. Huang, L. Zhang, M. He, S. Xu, D. Sun, X. Jiang, Moderate bacterial etching allows scalable and clean delamination of $g\text{-}C_3N_4$ with enriched unpaired electrons for highly improved photocatalytic water disinfection, ACS Appl. Mater. Interfaces 10 (2018) 13796–13804.
[20] Y. Xu, Y. Gong, H. Ren, W. Liu, L. Niu, C. Li, X. Liu, In situ structural modification of graphitic carbon nitride by alkali halides and influence on photocatalytic activity, RSC Adv. 7 (2017) 32592–32600.
[21] M. Zhang, Y. Duan, H. Jia, F. Wang, L. Wang, Z. Su, C. Wang, Defective graphitic carbon nitride synthesized by controllable co-polymerization with enhanced visible light photocatalytic hydrogen evolution, Catal. Sci. Technol. 7 (2017) 452–458.
[22] C. Zhou, X. Sun, J. Yan, B. Chen, P. Li, H. Wang, J. Liu, X. Dong, F. Xi, Thermo-driven catalytic degradation of organic dyes by graphitic carbon nitride with hydrogen peroxide, Powder Technol. 308 (2017) 114–122.
[23] Y. Gao, Y. Zhu, L. Lyu, Q. Zeng, X. Xing, C. Hu, Electronic structure modulation of graphitic carbon nitride by oxygen doping for enhanced catalytic degradation of organic pollutants through peroxymonosulfate activation, Environ. Sci. Technol. 52 (2018) 14371–14380.
[24] Z. Zhao, Y. Ma, J. Fan, Y. Xue, H. Chang, Y. Masubuchi, S. Yin, Synthesis of graphitic carbon nitride from different precursors by fractional thermal polymerization method and their visible light induced photocatalytic activities, J. Alloys Compd. 735 (2018) 1297–1305.
[25] Y. Wang, H. Wang, F. Chen, F. Cao, X. Zhao, S. Meng, Y. Cui, Facile synthesis of oxygen doped carbon nitride hollow microsphere for photocatalysis, Appl. Catal. B: Environ. 206 (2017) 417–425.
[26] S. Kang, M. He, M. Chen, J. Wang, L. Zheng, X. Chang, H. Duan, D. Sun, M. Dong, L. Cui, Ultrafast plasma immersion strategy for rational modulation of oxygen-containing and amino groups in graphitic carbon nitride, Carbon 159 (2020) 51–64.
[27] J. Yan, X. Han, J. Qian, J. Liu, X. Dong, F. Xi, Preparation of 2D graphitic carbon nitride nanosheets by a green exfoliation approach and the enhanced photocatalytic performance, J. Mater. Sci. 52 (2017) 13091–13102.
[28] L. Cui, Y. Liu, X. Fang, C. Yin, S. Li, D. Sun, S. Kang, Scalable and clean exfoliation of graphitic carbon nitride in NaClO solution: enriched surface active sites for enhanced photocatalytic H_2 evolution, Green Chem. 20 (2018) 1354–1361.
[29] A. Diac, M. Focsan, C. Socaci, A.-M. Gabudean, C. Farcau, D. Maniu, E. Vasile, A. Terec, L.M. Veca, S. Astilean, Covalent conjugation of carbon dots with rhodamine B and assessment of their photophysical properties, RSC Adv. 5 (2015) 77662–77669.
[30] P. Qiu, C. Xu, H. Chen, F. Jiang, X. Wang, R. Lu, X. Zhang, One step synthesis of oxygen doped porous graphitic carbon nitride with remarkable improvement of photo-oxidation activity: role of oxygen on visible light photocatalytic activity, Appl. Catal. B: Environ. 206 (2017) 319–327.
[31] R. Tang, R. Ding, X. Xie, Preparation of oxygen-doped graphitic carbon nitride and its visible-light photocatalytic performance on bisphenol A degradation, Water Sci. Technol. 78 (2018) 1023–1033.
[32] Q. Dong, N. Mohamad Latiff, V. Mazánek, N.F. Rosli, H.L. Chia, Z. Sofer, M. Pumera, Triazine- and heptazine-based carbon nitrides: toxicity, ACS Appl. Nano Mater. 1 (2018) 4442–4449.
[33] J. Li, B. Shen, Z. Hong, B. Lin, B. Gao, Y. Chen, A facile approach to synthesize novel oxygen-doped $g\text{-}C_3N_4$ with superior visible-light photoreactivity, Chem. Commun. (Camb.) 48 (2012) 12017–12019.
[34] C. Lu, Y. Yang, X. Chen, Ultra-thin conductive graphitic carbon nitride assembly through van der waals epitaxy toward high-energy-Density flexible supercapacitors, Nano Lett. 19 (2019) 4103–4111.
[35] Y. Zeng, X. Liu, C. Liu, L. Wang, Y. Xia, S. Zhang, S. Luo, Y. Pei, Scalable one-step production of porous oxygen-doped $g\text{-}C_3N_4$ nanorods with effective electron separation for excellent visible-light photocatalytic activity, Appl. Catal. B: Environ. 224 (2018) 1–9.
[36] H. Zhang, Y. Huang, S. Hu, Q. Huang, C. Wei, W. Zhang, L. Kang, Z. Huang, A. Hao, Fluorescent probes for "off–on" sensitive and selective detection of mercury ions and l-cysteine based on graphitic carbon nitride nanosheets, J. Mater. Chem. 3 (2015) 2093–2100.
[37] N. Wang, H. Fan, J. Sun, Z. Han, J. Dong, S. Ai, Fluorine-doped carbon nitride quantum dots: ethylene glycol-assisted synthesis, fluorescent properties, and their application for bacterial imaging, Carbon 109 (2016) 141–148.
[38] L. Wang, Y. Li, X. Yin, Y. Wang, A. Song, Z. Ma, X. Qin, G. Shao, Coral-like-structured Ni/C_3N_4 composite coating: an active electrocatalyst for hydrogen evolution reaction in alkaline solution, ACS Sustain. Chem. Eng. 5 (2017) 7993–8003.
[39] C. Wang, H. Fan, X. Ren, J. Ma, J. Fang, W. Wang, Hydrothermally induced oxygen doping of graphitic carbon nitride with a highly ordered architecture and enhanced photocatalytic activity, ChemSusChem 11 (2018) 700–708.
[40] Y. Zhang, J. Gao, Z. Chen, A solid-state chemical reduction approach to synthesize graphitic carbon nitride with tunable nitrogen defects for efficient visible-light photocatalytic hydrogen evolution, J. Colloid Interface Sci. 535 (2019) 331–340.
[41] C. Liu, H. Huang, W. Cui, F. Dong, Y. Zhang, Band structure engineering and efficient charge transport in oxygen substituted $g\text{-}C_3N_4$ for superior photocatalytic hydrogen evolution, Appl. Catal. B: Environ. 230 (2018) 115–124.
[42] Y.A. Workie Sabrina, T. Imae, M.P. Krafft, Nitric oxide gas delivery by fluorinated poly(Ethylene glycol)@Graphene oxide carrier toward pharmacotherapeutics, ACS Biomater. Sci. Eng. 5 (2019) 2926–2934.
[43] F. Fina, S.K. Callear, G.M. Carins, J.T.S. Irvine, Structural investigation of graphitic carbon nitride via XRD and neutron diffraction, Chem. Mater. 27 (2015) 2612–2618.
[44] X. Yuan, K. Luo, Y. Wu, J. He, Z. Zhao, D. Yu, Investigation on the stability of derivative melam from melamine pyrolysis under high pressure, Nanomaterials (Basel) 8 (2018).

[45] K. Akaike, K. Aoyama, S. Dekubo, A. Onishi, K. Kanai, Characterizing electronic structure near the energy gap of graphitic carbon nitride based on rational interpretation of chemical analysis, Chem. Mater. 30 (2018) 2341–2352.
[46] C.A. Davis, K. McNeill, E.M.-L. Janssen, Non-singlet oxygen kinetic solvent isotope effects in aquatic photochemistry, Environ. Sci. Technol. 52 (2018) 9908–9916.
[47] N. Tian, Y. Zhang, C. Liu, S. Yu, M. Li, H. Huang, g-C_3N_4/$Bi4O_5I_2$ 2D–2D heterojunctional nanosheets with enhanced visible-light photocatalytic activity, RSC Adv. 6 (2016) 10895–10903.
[48] Y.-H. Chiu, T.-F.M. Chang, C.-Y. Chen, M. Sone, Y.-J. Hsu, Mechanistic insights into photodegradation of organic dyes using heterostructure photocatalysts, Catalysts 9 (2019), https://doi.org/10.3390/catal9050430.
[49] P. Qiu, J. Yao, H. Chen, F. Jiang, X. Xie, Enhanced visible-light photocatalytic decomposition of 2,4-dichlorophenoxyacetic acid over $ZnIn_2S_4$/g-C_3N_4 photocatalyst, J. Hazard. Mater. 317 (2016) 158–168.
[50] K. Del Ángel-Sanchez, O. Vázquez-Cuchillo, A. Aguilar-Elguezabal, A. Cruz-López, A. Herrera-Gómez, Photocatalytic degradation of 2,4-dichlorophenoxyacetic acid under visible light: effect of synthesis route, Mater. Chem. Phys. 139 (2013) 423–430.
[51] U.G. Akpan, B.H. Hameed, Photocatalytic degradation of 2,4-dichlorophenoxy-acetic acid by Ca–Ce–W–TiO_2 composite photocatalyst, Chem. Eng. J. 173 (2011) 369–375.
[52] S. S, K.L. Nagashree, T. Maiyalagan, G. Keerthiga, Photocatalytic degradation of 2,4-dichlorophenoxyacetic acid - a comparative study in hydrothermal TiO_2 and commercial TiO_2, Appl. Surf. Sci. 449 (2018) 371–379.
[53] M. Abdennouri, A. Elhalil, M. Farnane, H. Tounsadi, F.Z. Mahjoubi, R. Elmoubarki, M. Sadiq, L. Khamar, A. Galadi, M. Baâlala, M. Bensitel, Y. El hafiane, A. Smith, N. Barka, Photocatalytic degradation of 2,4-D and 2,4-DP herbicides on Pt/TiO_2 nanoparticles, J. Sauidi. Chem. Soc. 19 (2015) 485–493.
[54] S.-M. Lam, J.-C. Sin, A.Z. Abdullah, A.R. Mohamed, Investigation on visible-light photocatalytic degradation of 2,4-dichlorophenoxyacetic acid in the presence of MoO_3/ZnO nanorod composites, J. Mol. Catal. A.-Chem. 370 (2013) 123–131.
[55] R. Nagaraja, N. Kottam, C.R. Girija, B.M. Nagabhushana, Photocatalytic degradation of Rhodamine B dye under UV/solar light using ZnO nanopowder synthesized by solution combustion route, Powder Technol. 215-216 (2012) 91–97.